

## **Time-Domain Finite Element Modeling of 3D Integrated Optical Devices**

**G. Wojcik, J. Mould Jr.**, *Weidlinger Associates*, 4410 El Camino Real, Los Altos, CA 94022 {(415) 949-3010}; **L.C. West**, 4G518, *AT&T Bell Labs*, Crawfords Corner Rd., Holmdel, NJ 01133 {(908) 949-8715}

### **Introduction**

As integrated optical devices become more sophisticated, so does the experimentation and analysis required to design them. By augmenting conventional experiments with rigorous computer modeling we can lower costs, shorten schedules, and provide faster, more accurate predictions. Discrete modeling codes using finite differences or finite elements are the most general, albeit expensive. Nonetheless, they are competitive today by virtue of simple, robust algorithms and modern workstations that put near-supercomputer capabilities on the desktop.

In support of computer modeling this paper demonstrates the practicality of time-domain finite element codes for simulating 2D and 3D devices on UNIX work-stations. We describe EMFlex, a finite element wave solver for large-scale electro-magnetic simulations, and apply it to highly confining dielectric waveguides in 3D routing and 2D grating couplers. EMFlex was originally developed for optical lithography and metrology studies<sup>1,2</sup>, funded in part by the NSF and SEMATECH.

### **Time-Domain Finite Elements**

We seek discrete solutions of Maxwell's equations in heterogeneous dielectric and semiconductor domains. Solving in the frequency-domain couples fields at all points in space and yields large systems of equations. A more practical approach is to integrate Maxwell's equations in the time-domain using finite differences. The equations' fundamental hyperbolicity decouples points separated by  $\Delta x$  if time step  $\Delta t$  is less than  $\Delta x/c$ , where  $c$  is the local speed of light. The discrete problem is then solved locally at each time step—by summing nodal contributions from nearest neighbors and integrating each node independently using a leapfrog scheme. "Lumping" permittivity at the nodes yields further simplification. This approach eliminates the large system of frequency-domain equations and yields a simple, fast algorithm that is well suited to pipelined or parallel computer architectures.

There are two standard methods for spatial discretization of Maxwell's equations, finite differences and finite elements. Finite differences<sup>3</sup> are the oldest and the most efficient for structurally simple models. Finite elements are newer and better suited to structurally complex models, but increase the floating point operation count. They also yield simpler (nonstaggered) field sampling and include nonlinear material behavior more readily. The dominance of finite elements in the commercial sector (thermal, structures, fluids, EM) is due to geometric adaptability and modeling ease. Speed turns out to be a secondary issue in most cases.

A critical issue for discrete solvers is grid truncation error caused by spurious reflections at the model's artificial boundaries. Radiation conditions are necessary to reduce this error. In time-domain analysis these are usually local relations among nodal boundary values derived from the paraxial wave equation<sup>4</sup>. However, higher order implementations tend to degrade in 3D vector domains. Also, the local phase velocity is required. A better approach is based on the formalism outlined below.

$$\dot{\underline{E}}_n \equiv \frac{1}{\varepsilon} \frac{\partial(\underline{n} \times \underline{H})}{\partial n} \quad , \quad \frac{\partial}{\partial n} = S_n \frac{\partial}{\partial t} \quad \Rightarrow \quad \dot{\underline{E}}_n = -\text{sign} \left[ \frac{\partial \underline{E}_n}{\partial n} \right] \sqrt{\frac{1}{\varepsilon} \left| \frac{\partial \underline{E}_n}{\partial n} \right| |\underline{n} \times \dot{\underline{H}}|}$$

The first equation rewrites the normal component of Maxwell's equation on  $\mathbf{E}$  (similarly for  $\mathbf{H}$ ). The second is the plane wave jump condition projected onto the boundary normal, where  $S_n$  is the unknown normal component of slowness. Applying this jump condition to the two sides of the first equation and eliminating  $S_n$  yields the third equation, giving the time derivative of the normal electric field in terms of its normal derivative and the time derivative of the magnetic field. Tangential conditions may be derived in the conventional fashion, by differencing nodal values for example. The important point is that these boundary conditions do not involve the local speed of light and they perform as well as 4<sup>th</sup> order paraxial conditions but with less computational overhead. They are unique in that nonlinear material behavior is permitted at the radiating boundary.

In addition to its fundamental wave solving capabilities, a practical code needs various pre- and post-processing options, both quantitative and graphical. For example, pre-processing includes calculating "illumination" conditions representing the optical field incident from outside the model, e.g., plane waves, Gaussian beams, waveguide modes, etc. To make these compatible with the radiation conditions, EMFlex does exact phase velocity matching using dispersion analysis of the discrete equations on the boundary. Post-processing includes automated amplitude and phase extraction from the steady state time-domain solution, scattered field extraction, far-field extrapolation, plane wave decomposition, and other means of characterizing device performance, e.g., modal mixes in a 3D waveguide. In addition, there is a complete graphical display and PostScript capability for interactive plotting of time histories, field snapshots, and movies.

## Model Problems

Our interest is integrated optical waveguides with high index of refraction contrast between the guide and surrounding dielectrics. Such high-contrast may allow unprecedented optical component and wiring densities, comparable to electronic integration, with compaction two orders of magnitude smaller than typical integrated optics. Unfortunately, this approach has not received much attention because fabrication of devices for 1 micron light pushes the outer limits of optical lithography. Also, practical analysis of these devices is difficult if not impossible using perturbation, paraxial, and ray theories. This causes us to question design rules and how they reflect limitations of traditional analysis methods.

Initial realization of these devices has been in the mid-IR (10 microns) with Ge waveguides ( $n=4.0$ ) on GaAs ( $n=3.27$ ). A typical waveguide is 1.75 microns high and 3.0 microns wide. The mid-IR region is considered ideal for device development because of fabrication ease, good dimensional control, and relative surface smoothness. Also, many practical nonlinear and electro-optic elements (detectors, modulators, logic, etc.) can be made with intersubband transitions<sup>5</sup> in the mid-IR. With advances in lithographic resolution, we expect these concepts to be useful in near-IR (1 micron) too, e.g., sizes should scale with wavelength to 0.2-0.3 microns.

Our model problems concern low-loss routing of optical signals through a circuitous waveguide and coupling off-chip beams into on-chip waveguide modes. In particular, we use EMFlex to calculate TM modes in 3D waveguides, propagation through a tight waveguide turn, and scattering from a single tooth in a 2D waveguide. Our eventual objective is to

optimize designs for a given set of nominal dimensions and layout constraints. These calculations were done on an IBM RS/6000 Model 350 workstation with 64 megabytes of memory.

Mode shapes are calculated in the time-domain by applying an approximate TM mode to one end face of a long 3D symmetric model with radiation or symmetry conditions on the other faces. The model is 10.5 microns deep, 9 microns wide, and 60 microns long ( $71 \times 61 \times 406 \approx 1.76$  million nodes). Shape of the stable mode that arrives approximately 12 wavelengths from the illuminated end is then measured. Thus, we use the finite element model as a waveguide filter. These experiments are done for a number of cross-sections and the effective index is calculated to insure that modes are trapped. Leaky modes are also apparent by their gradual amplitude decay. Mode shapes calculated in this manner are illustrated in Figure 1 for a  $1.75 \times 3.0$  micron cross-section. The effective index is 3.33. Waveguide height is the critical dimension in these 3D experiments. For example, a  $1.65 \times 3.0$  micron cross-section is leaky although the  $1.65 \times \infty$  micron case (slab) is not.

To illustrate modeling of waveguide routing we use the above cross-section and model a 7.5 micron radius turn (2.5 wavelengths). The TM mode shape is applied as a boundary condition on the input face with radiation conditions on the other five faces. Snapshots of the field are shown in Figure 2 after the mode has traversed the bend and a few waves have been absorbed at the other face. The model is 15 microns square and 10.5 microns deep ( $101 \times 101 \times 71 \approx 724,000$  nodes).

Our basis for investigating grating couplers is scattering from a single tooth. This is used to design arbitrary output beam profiles. The 2D Ge waveguide is 1.75 microns thick over GaAs. The tooth is 1.5 microns wide and etched into the waveguide from above. The 2D model is 24.4 microns deep and 150 microns long ( $138 \times 1001 \approx 138,000$  nodes). Illumination and boundary conditions are similar to those described above. Results for the fundamental TM mode incident from the left are illustrated in Figure 3. This shows amplitudes of the vertical (top) and horizontal (bottom) electric field components in the neighborhood of a 0.477 micron tooth, and a plot of reflected amplitude coefficient, transmitted amplitude coefficient, and scattered power coefficient for tooth depths from 0. to 1.75 microns (full penetration).

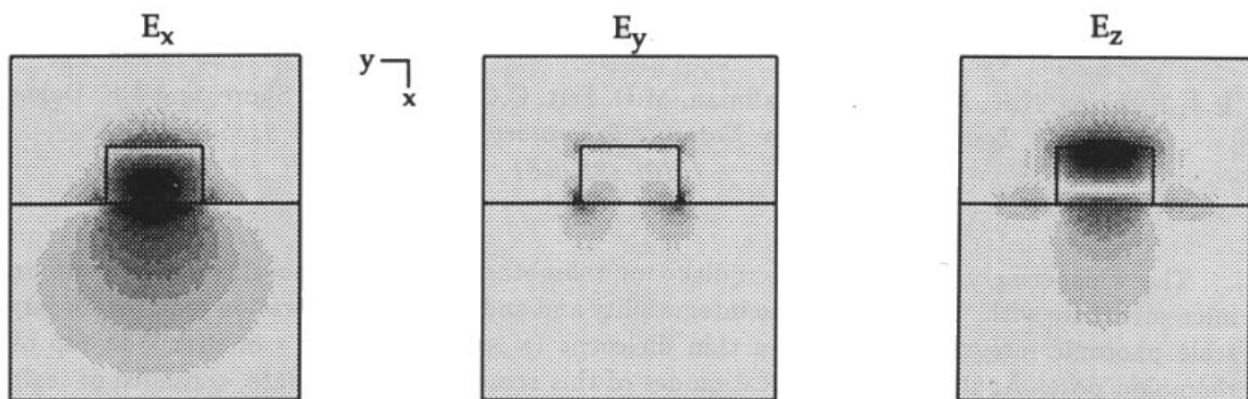


Figure 1. Fundamental TM mode shapes in a  $1.75 \times 3.0$  micron Ge ( $n=4.0$ ) waveguide on GaAs ( $n=3.27$ ). Free-space wavelength is 10 microns and effective index of the mode is 3.33. The smaller  $E_y$  and  $E_z$  fields are scaled by a factor of 2.0 over  $E_x$ .

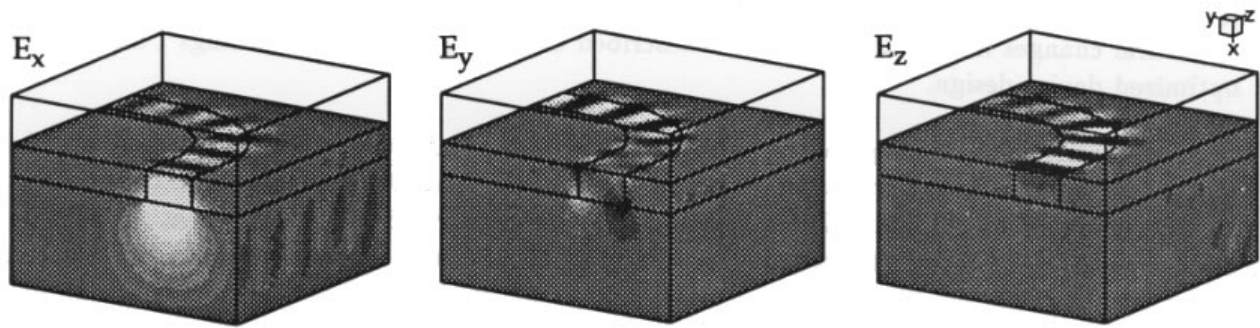


Figure 2. Fundamental TM mode propagation in the waveguide of Figure 1 with a 7.5 micron radius turn. The mode is applied on the left, front face and absorbed on the left, rear face. The smaller  $E_y$  and  $E_z$  fields are scaled by a factor of 1.6 over  $E_x$ .

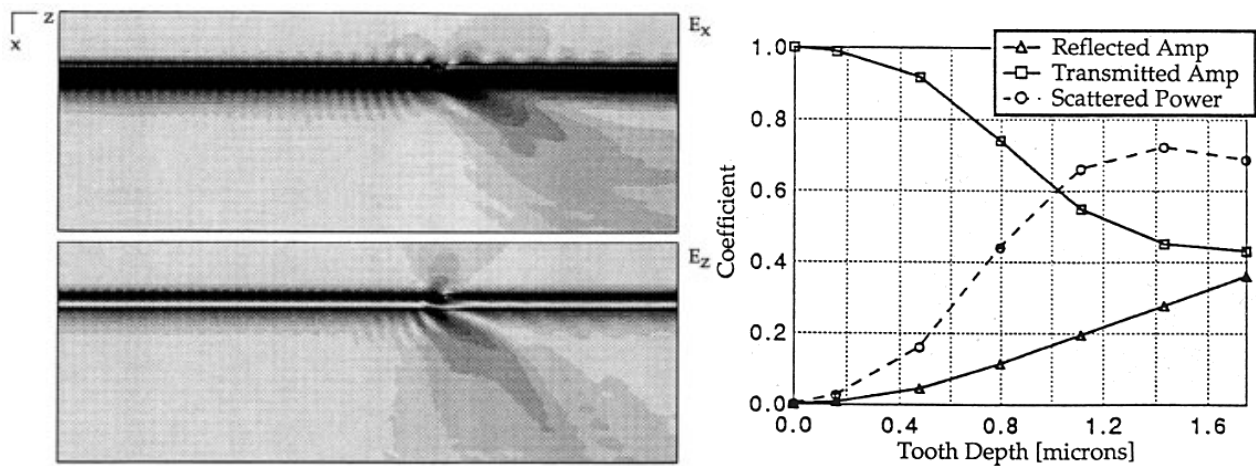


Figure 3. Scattering from a 1.5 micron wide tooth in a 1.75 micron Ge slab waveguide over GaAs. Fields scattered from a 0.477 micron deep tooth are shown on the left. Scattering coefficients as a function of tooth depth are plotted on the right.

## Conclusions

We have shown that workstation-based computer modeling of 3D high-contrast optical devices is practical. There are limitations of course, on problem size and complexity, wavelength versus feature size (subscale roughness), and boundary conditions—but none appear insurmountable. General modeling codes like EMFlex that are tailored to facilitate numerical experimentation will prove valuable to the designer and experimentalist, particularly as desktop computing power increases.

Concerning the high-contrast wafer-scale models described here, it is clear that complete performance information can be obtained in regimes where more classical approximations fail utterly. We know how to fabricate these devices but lack the knowledge to design them. Tailored modeling codes can help develop the necessary knowledge base and facilitate new classes of integrated optical devices.

## References

1. G. Wojcik, D. Vaughan, and L. Galbraith, "Calculation of light scatter from structures on silicon surfaces," **SPIE Vol. 774**, *Lasers in Microlithography* (1987).
2. G. Wojcik, et. al, "Numerical simulation of thick line width measurements by reflected light," **SPIE Vol. 1464**, *IC Metrology, Inspection & Process Control* (1991).
3. K.S. Yee, "Numerical solution of initial boundary value problems involving Maxwell's equations in isotropic media," *IEEE Trans. Antennas Prop.*, **AP-14**, pp. 302-307 (1966).
4. B. Engquist, A. Majda, "Absorbing boundary conditions for the numerical simulation of waves," *Math. Comp.*, **31**, pp. 629-651 (1977).
5. L.C. West, "Picosecond Integrated Optical Logic," *Computers*, **20**, pp. 34-46 (1987).